Two-Phase Flow Analysis in Multi-Channel

Man Yeong Ha*
School of Mechanical Engineering, Pusan National University,
San 30, Jangjeon-Dong, Kumjeong-Ku, Pusan 609-735, Korea
Cheol Hwan Kim, Yong Won Jung, Seong Geun Heo
LG Elecrtronics DAC Lab.,
391-2, Gaeumjeong-Dong, Changwon City, Gyeongnam 641-711, Korea

We carried out numerical studies to investigate the single- and two-phase flow characteristics in the single- and multi-channels. We used the finite volume method to solve the mass and momentum conservation equations. The volume of fluid model is used to predict the two-phase flow in the channel. We obtained the distribution of velocity fields, pressure drop and air volume fraction for different water mass flow rates. We also calculated the distribution of mass flow rates in the multi-channels to understand how the flow is distributed in the channels. The calculated results for the single- and two-phase flow are partly compared with the present experimental data both qualitatively and quantitatively, showing relatively good agreement between them. The numerical scheme used in this study predicts well the characteristics of single- and two-phase flow in a multi-channel.

Key Words : Two-phase Flow, Multi-branched Multi-channel, Numerical Analysis, VOF (Volume of Fluid)

Nomenclature

D : Diameter [m]
L : Channel length [m]
P : Pressure [Pa]
Re : Reynolds number, $\rho V_{in} D_h / \mu$
Q : Flow rate [m^3/s]
V : Velocity [m/s]
ρ : Density [kg/m^3]
μ : Viscosity [Ns/m^2]

Subscript

h : Hydraulic
in : Inlet condition
ref : Reference condition

* Corresponding Author,
E-mail : myha@pusan.ac.kr
TEL : +82-51-510-2440; **FAX** : +82-51-512-9835
School of Mechanical Engineering, Pusan National University, San 30, Jangjeon-Dong, Kumjeong-Ku, Pusan 609-735, Korea. (*Manuscript* **Received** April 15, 2005; **Revised** March 23, 2006)

1. Introduction

Micro-fluidics is a rapidly developing area of research with great potential for a wide range of applications in many fields. One area of micro-fluidics is gas-liquid two-phase flow in micro-channels. There has been and are still going on many researches on fluid flow, but most of these researches are related with the single channel though two-phase fluid flow and pressure drop in multi-channel are used in the real applications. Thus the prediction of the fluid flow and pressure drop characteristics considering two-phase flow is more important. And it is also very important to predict correctly the distribution of the mass flow rate because it determines the overall performance of the system.

There have been many studies to investigate two-phase flow in the channel. They investigated the two-phase flow pattern formed in the channel and as a result its pressure drop characteristics,

which were different from the single-phase flow. A large part of previous studies considered two-phase flow patterns formed in large-diameter channel using air-water or air-oil mixture (Alves, 1954).

There have been increasing interests for the two-phase flow in the small-size channel with rapid development of MEMS technology and its application to real problems recently. Coleman and Garimella (1999) found that the diameter and cross-sectional shape of channel could have significant effects on the two-phase flow pattern formed in the channel when $D_{in}<1$ mm. Hirt and Nichols (1981) suggested the VOF (volume-of-fluid) method to predict two-phase flow. VOF was considered as an effective computational scheme to solve two-phase flow problems with complicated phase interface. Elghobash and Aou-Arab (1983) used two-equation turbulence model to analyze the two-phase jet flow. Ashgriz and Poo (1991) suggested the interface tracking scheme to calculate void fraction from the slope and advection of element. Most of these studies investigate the two-phase flow characteristics in the single channel.

In the present study, we investigated the single- and two-phase flow and its pressure drop characteristics in the mini-sized single- and multi-channel. Multi-channel has a distributor and collector. The calculation results for the pressure drop in the single channel are compared with experimental data. In the multi-branched and stacked multi-channel study, we calculated the bubble dynamics and mass flow rate through each channel consisting of the multi-channel as a function of time for different inlet water mass flow rate.

2. Experimental Methodology

Figure 1 shows a schematic diagram of experimental apparatus to measure single- and two-phase flows in the single channel and single-phase flows in the five-branched multi-channel. The water supply loop consists of a constant temperature water bath with a pump, a mass flow meter and a needle valve. The air supply loop includes a pressurized air bomb, a mass flow meter and a needle valve. The test section is made of bronze and acrylic plates, and it has a single and

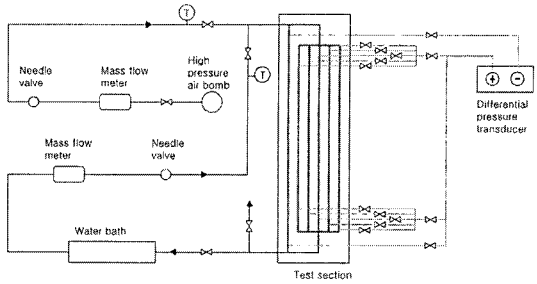

(a) Schematic diagram

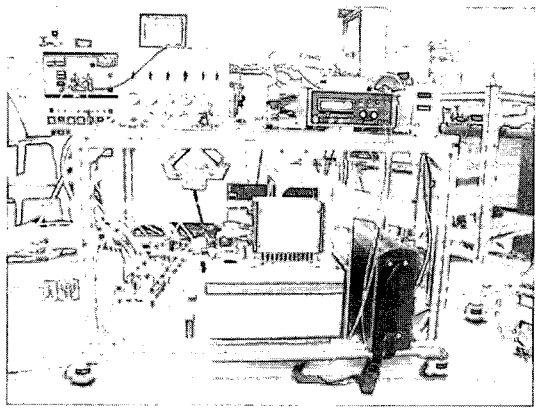

(b) Photo

Fig. 1 A schematic diagram and photo of experimental apparatus to measure single- and two- phase flows in the single-channel and single-phase flows in the five-branched multi-channel

five-branched channels as shown in Fig. 1. Two different types of pressure transducers are used to measure the pressure difference of air and water flow. Temperature is measured by RTD sensors. Data are collected and sent to data acquisition system by RS 232C port.

Figure 2 shows a schematic diagram of experimental apparatus to measure two-phase flows in the multi-branched multi-channel. The experimental equipment consists of different parts of water bath, fuel and air supply, electric load and hood. The capacity of stainless water bath with heater and motor is 20 liters. The water bath controls the fuel temperature properly by maintaining the water temperature uniformly. Fuel is supplied to the stack using a pump from the fuel tank whose diameter and height are 200 mm and 300 mm, respectively. We install the pressure gauges and thermometers at the inlet and the

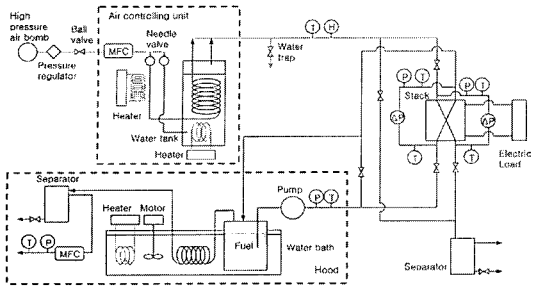

(a) Schematic diagram

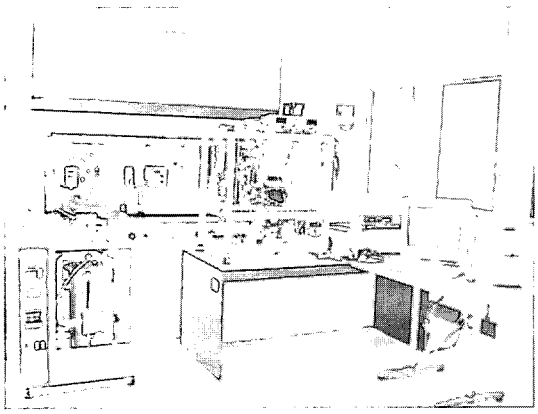

(b) Photo

Fig. 2 A schematic diagram and photo of experimental apparatus to measure two-phase flows in a multi-channel

outlet of stack to measure the fuel properties. The fuel used in the present experiment is the solution of borohidride and the temperature of fuel at the inlet is 60 ℃. After the reaction is done at the stack, the residue of fuel goes back to the top of the fuel tank and is separated into the gas and liquid. The liquid fuel is cooled down at the water bath and re-circulated to the stack. The gas fuel is also cooled down while passing through the spiral tube whose diameter and length are 6.4 mm and 1.5 m, respectively, and reaches to the separator. The gas fuel separated at the separator is finally exhausted to the atmosphere through the hood. The air is supplied from the high-pressure air bomb and its pressure is reduced by a reducing valve. The flow rate of air is controlled using the flow meter. The temperature and humidity of air is controlled while it passes through the air control unit consisting of heater, spiral tube whose diameter and length are 6.4 mm and 1.5 m, respectively, and water tank. After the air passes through the air control unit, it reaches to the stack and reacts with fuel. The temperature and humidity of air at the inlet of stack are 60℃ and 100%, respectively. After the air is used for reaction in the stack, it goes to the separator and is separated to the dry air and water. The 500 W electric load with the fixed current is used to measure the performance of stack.

3. Numerical Methodology

In order to investigate the two-phase flow in the multi-channel, the governing equations are defined based on the VOF (Volume of Fluid) formulation which relies on the fact that two or more fluids (or phases) are not interpenetrating. The continuity and momentum conservation equations based on the VOF formulation are.

$$\frac{\partial}{\partial t}(\alpha_q\rho_q)+\nabla\cdot(\alpha_q\rho_q\vec{v}_q)=0 \tag{1}$$

$$\frac{\partial}{\partial t}(\rho\vec{v})+\nabla\cdot(\rho\vec{v}\vec{v}) =-\nabla p+\nabla\cdot[\mu(\vec{\nabla}\vec{v}+\Delta\vec{v}^{T})]+\rho g+\vec{F} \tag{2}$$

where α_q represents the q-th fluid's volume fraction in the cell and the following three conditions are possible :

- $\alpha_q=0$: the cell is empty (of the q-th fluid)
- $\alpha_q=1$: the cell is full (of the q-th fluid)
- $0<\alpha_q<1$: the cell contains the interface between the q-th fluid and one or more fluids.

The volume-fraction-averaged density and viscosity takes on the following form :

$$\rho=\sum\alpha_q\rho_q,\ \mu=\sum\alpha_q\mu_q \tag{3}$$

In order to consider the turbulence quantities, the two-equation (k-ε) model is used and the turbulence variables are shared by the phases throughout the field. These governing equations are solved numerically by the finite volume method.(Patankar, 1980)

Figure 3 shows the schematic diagram to show the geometries used in the present study to calculate the single- and two-phase flows in the single- and multi-channels based on the experimental apparatuses shown in Figs. 1 and 2. The square

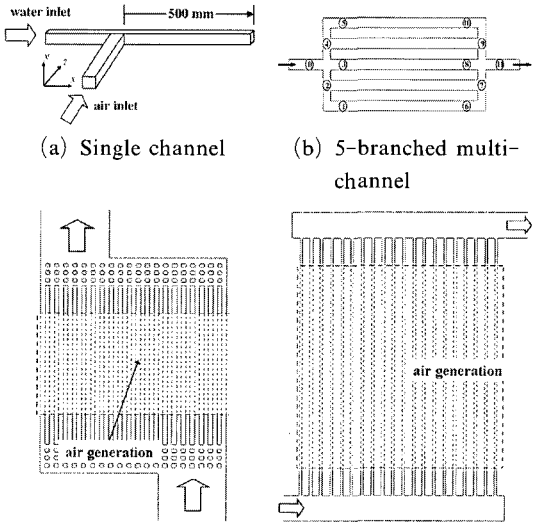

(a) Single channel (b) 5-branched multi-channel

(c) Multi-branched multi-channel (d) Stacked mult-channel

Fig. 3 Schematic diagram to show the geometries used in the present study to calculate the single- and two-phase flows in the single- and multi-channels based on the experimental apparatuses shown in Figs. 1 and 2

cross-sectional hydraulic diameter and the length of the single channel and five-branched multi-channel are 5 mm and 500 mm, respectively. The hydraulic diameter of multi-branched multi-channel and stacked multi-channel is 2 mm.

4. Results and Discussion

4.1 Single- and two-phase flow in the single channel

Figure 4 shows the pressure drop for the single-phase flow in the single-channel as a function of Reynolds number for different working fluids of air and water. The measured points of pressure in the single channel are 20 mm and 480 mm from the inlet. The present computational results for the friction factor are compared with the Moody chart and present experimental data, showing the good agreement among them.

Figure 5 shows the contours of air volume fraction obtained form the present calculation for the air-water two-phase flow in the single channel at different times of 1 and 2 sec. The inlet velocity of air and water is 1.66 m/s and 0.04 m/s, respec-

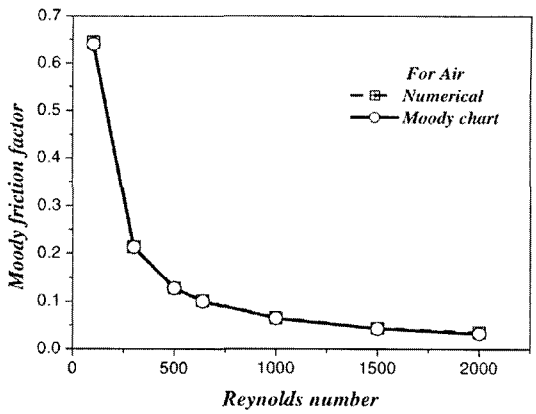

(a) Air

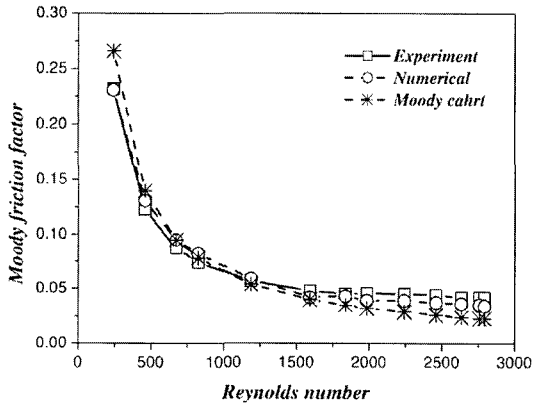

(b) Water

Fig. 4 Moody friction factor as a function of Reynold number for the single-phase flow in the single-channel

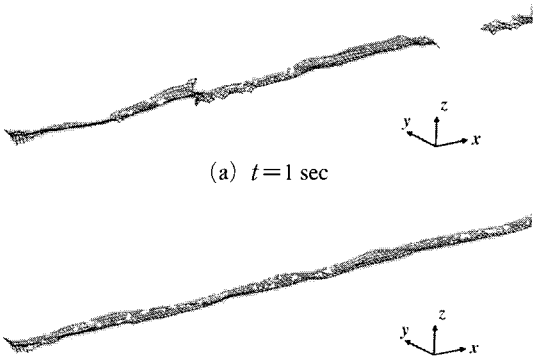

(a) $t=1$ sec

(b) $t=2$ sec

Fig. 5 Contours of air volume fraction for two-phase flow in the single-channel

tively. The air flows at the upper part of channel due to the buoyancy effects, whereas water flows

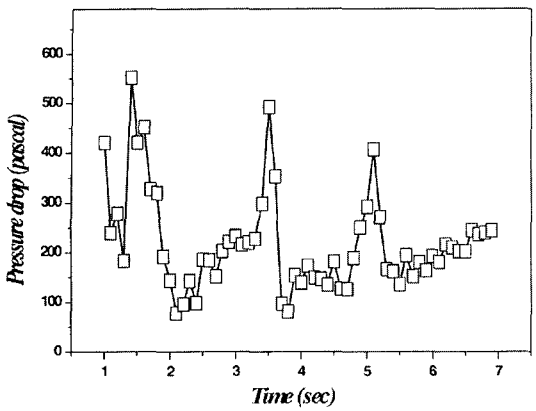

Fig. 6 Time history of pressure drop for the two-phase flow in the single-channel

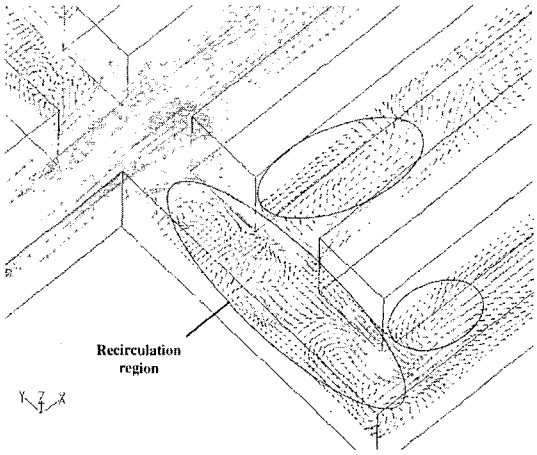

Fig. 7 Distribution of single-phase flow at the inlet region of five-branched multi-channel Flow

at the lower part of channel. We can also observe the development of phase interface between air and water from the irregular to the smooth shape, as time goes on from $t=1$ sec to $t=2$ sec.

Figure 6 shows the time history of pressure drop obtained from the present calculation for the two phase flow in the single channel. The points used to calculate the pressure drop are 20 mm apart from the intersection of air and water inlet. The pressure drop oscillates regularly with a period of 1.5 sec after the initial transient state corresponding to about 2 seconds. The time-averaged pressure drop obtained form the present calculation is about 200 Pa. The measured time-averaged pressure drop obtained from the present experiment is about 260 Pa. This result shows that the present calculation using VOF model predicts the pressure drop reasonably well for the pressure drop for the two-phase flow in the single channel.

4.2 Single phase flow in the five-branched multi-channel

Figure 7 shows the distribution of single-phase flow at the inlet region of five-branched multi-channel. The flow is very complex due to the geometrical complexity and we can observe the big re-circulating flow at the inlet. This re-circulating flow at the inlet makes the flow through each channel non-uniform and the pressure drop at the inlet very high. This result shows that this geometry with five-branched channel is not a good

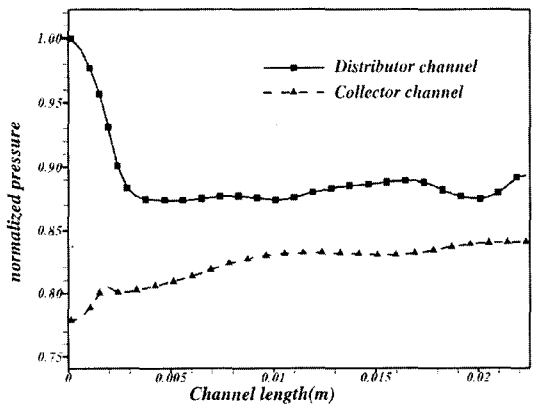

Fig. 8 The normalized pressure distribution in the distributor and collector of five-branched multi-channel

design for the uniform flow distribution through the channel. Thus, the pressure distribution in the distributor and collector is not uniform as shown in Fig. 8. The normalized pressure in Fig. 8 is defined as

$$p^* = \frac{p - p_{ref}}{p_{\max} - p_{ref}} \tag{4}$$

where P_{ref} and $P_{\max}$ represent the reference pressure at the inlet of channel and the maximum pressure at the outlet of channel.

Figure 9 shows the normalized pressure distribution along the channel located at the center. The pressure decreases linearly from the inlet of multi-channel to the inlet of distributor. The pres-

sure increases in the distributor due to the sudden expansion. The pressure decreases again linearly along the center channel. The pressure decreases very rapidly from the outlet of collector to the exit of multi-channel due to sudden contraction.

Figure 10 shows the friction factor for the single phase flow calculated at different positions shown in Fig. 3 for different Reynolds numbers of 1500, 2300, 3000 and 35000. The fiction factor is defined as

$$f=\frac{\Delta p}{2\rho V^2}\frac{D_h}{L} \tag{5}$$

The calculated results are compared with the measured data in the present study. There are some discrepancies between numerical and experimental results in the distributor channel due to complex flow pattern with re-circulating flow. However, the calculated results agree well with the measured ones at the fully developed exit region.

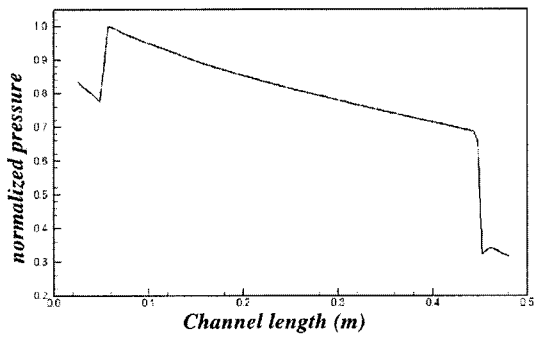

Fig. 9 Normalized pressure distribution along the channel located at the center

4.3 Two-phase flow in the multi-branched multi-channel

Figure 11 shows the contours of air volume fraction at different times of 0.5 and 2.5 seconds and for different inlet water mass flow rates of

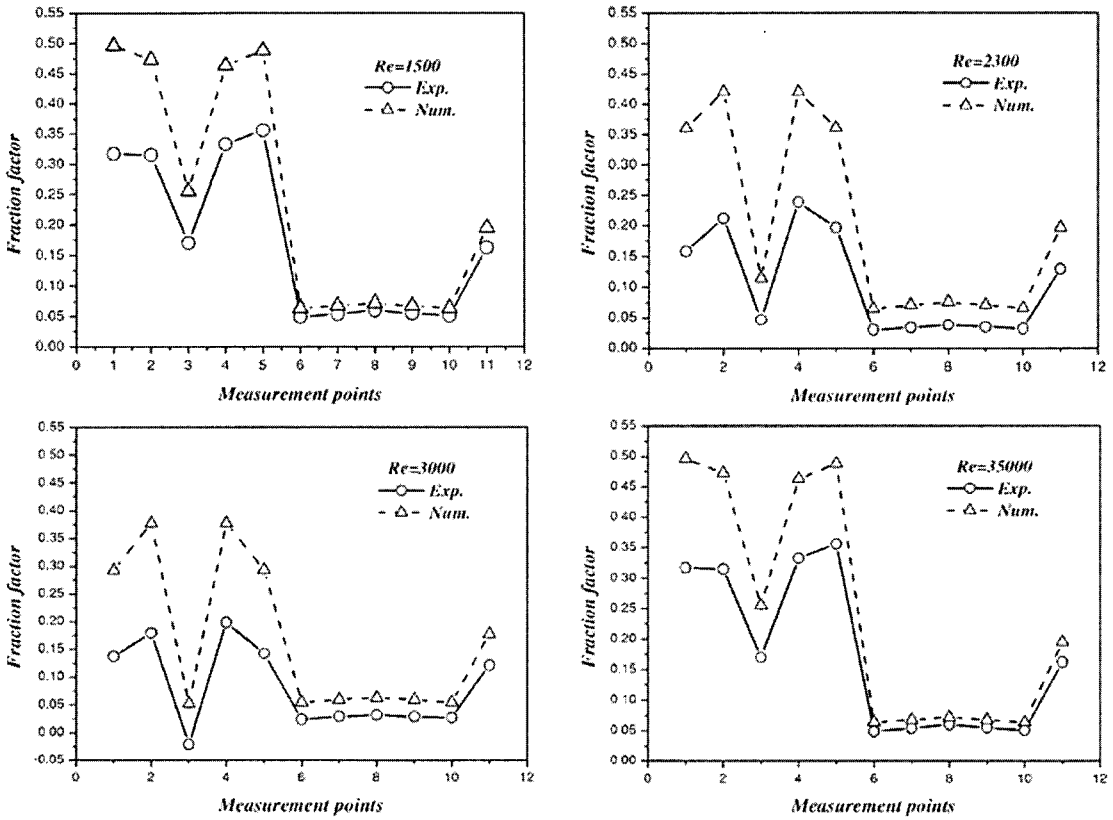

Fig. 10 Friction factor for the single phase flow calculated at different positions shown in Fig. 3 for different Reynolds numbers of 1500, 2300, 3000 and

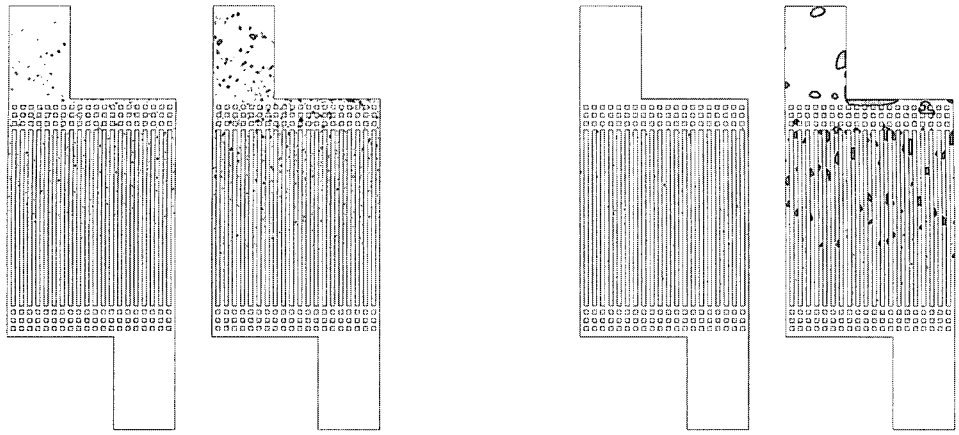

(a) $\dot{m}_{in,water}=1.67\times10^{-4}$ kg/s (b) $\dot{m}_{in,water}=8.32\times10^{-4}$ kg/s

Fig. 11 Contours of air volume fraction at different times of 0.5 and 2.5 seconds and for different inlet water mass flow rates of 1.67×10^{-4} and 8.32×10^{-4} kg/s

1.67×10^{-4} and 8.32×10^{-4} kg/s. The air is generated at a rate of 0.1 kg/m^{3}s in the channel which was initially filled with water, as shown in Fig. 3. When $t=0.5$s corresponding to the relatively earlier state, the small-sized air bubbles formed in the channels rise uniformly along the channel without any interference and agglomeration of air bubbles for different water mass flow rates of 1.67×10^{-4} and 8.32×10^{-4} kg/s. If the time is increased to 2.5 seconds, the small-sized air bubble becomes larger due to the interference and agglomeration of small-sized air bubbles. After $t=$ 2.5s, the two-phase flow in the channels does not depend much on time variation. When the water mass flow rate is 1.67×10^{-4} kg/s and $t=2.5$s, the size of agglomerated air bubble is relatively uniform and is not large enough to block the flow of water-air mixture. Thus the mass flow rate through each channel is almost uniform. However, if the water mass flow rate is increased to 8.32×10^{-4} kg/s at $t=2.5$s, the size of agglomerated air bubble becomes large enough to block the mixture flow. Due to the geometry of the present multi-channel, the biggest bubbles are formed around the center of upper wall of multi-channel by the accumulated agglomeration of air bubbles rising in the right side of multi-channel, resulting in the smallest mass flow rate along the channels around the center. The present simulation results for the two-phase flow distribution in the multi-channel represents well the flow visualization results qualitatively, as shown in Fig. 12.

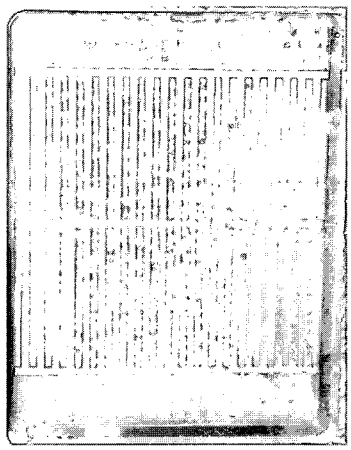

Fig. 12 A photo of flow visualization result in a multi-branched multi-channel

Figure 13 shows the ratio of mass flow rate in the channels for different times and for different water mass flow rates of 1.67×10^{-4} and 8.32×10^{-4} kg/s. The mass flow rate in the channels is normalized by that at the 11th channel from the left side of multi-channel. When the inlet water mass flow rate is 1.67×10^{-4} kg/s, the mass flow rate through channels during the initial period is not uniform but becomes almost uniform as time

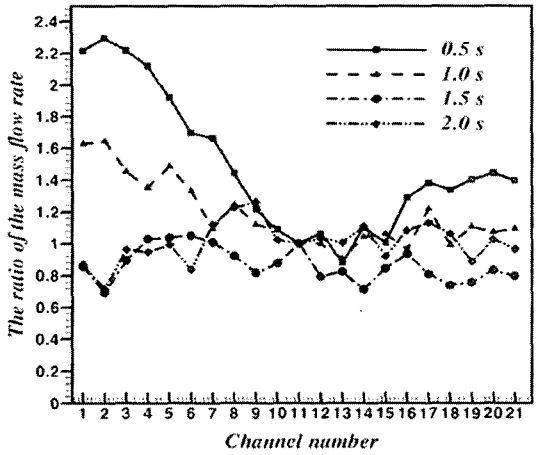

(a) $\dot{m}_{in,wader}=1.67\times10^{-4}$ kg/s

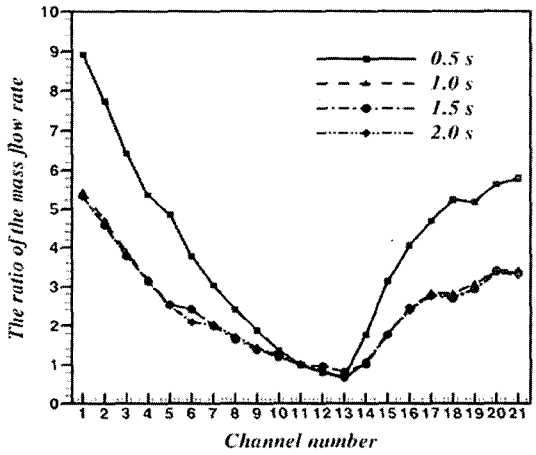

(b) $\dot{m}_{in,water}=8.32\times10^{-4}$ kg/s

Fig. 13 Ratio of mass flow rate in the channels for different times and for different water mass flow rates of 1.67×10^{-4} and 8.32×10^{-4} kg/s in the multi-branched multi-channel

goes on. However, if the inlet water mass flow rate is increased to 8.32×10^{-4} kg/s, the mass flow rate through channels is not uniform for all time. The mass flow rate through the channels around the center is much smaller than those located at the right and left-hand sides due to the reasons explained in Fig. 11. When $\dot{m}_{in,water}=8.32\times10^{-4}$ kg/s, the ratio of mass flow rate in different channel numbers for $t=2.0$s is the same as $t=1.5$s, meaning that the system reaches the steady state after $t=1.5$s. So we can not distinguish the differences in the ratio of mass flow rate in different channel numbers between $t=1.5$s and $t=2.0$s.

4.4 Two-phase flow in the stacked multi-channel

Figure 14 shows the contours of air volume fraction for different inlet water mass flow rates of 1.67×10^{-2} and 1.67×10^{-1} kg/s at $t=4$s. The air bubble dynamics in the stacked multi-channel is generally similar to that in the multi-branched multi- channel. The major difference is observed at the collector. If the inlet water mass flow rate is small, the air bubbles are agglomerated and stick to the upper wall of collector together and forms thick layer of air bubble along the upper wall in the collector. However, if the inlet water mass flow rate becomes larger, the air bubbles do not agglomerate and move independently to the outlet of collector due to larger inertia with increasing inlet water mass flow rate. Thus the ratio of mass flow rate in the stacked multi-channel is relativ-

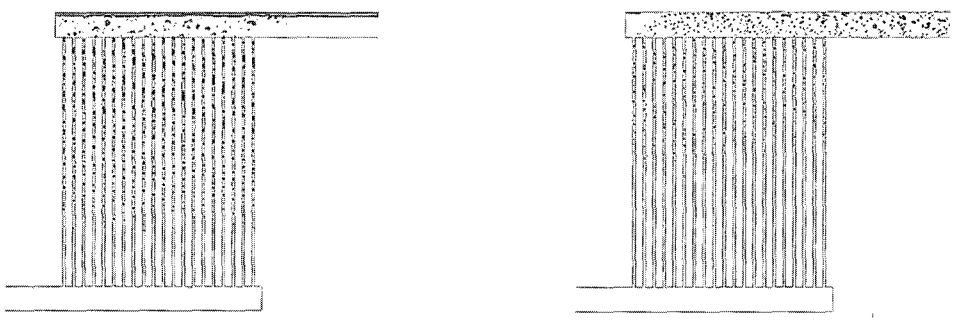

(a) $\dot{m}_{in,water}=1.67\times10^{-2}$ kg/s (b) $\dot{m}_{in,water}=1.67\times10^{-1}$ kg/s

Fig. 14 Contours of air volume fraction for different inlet water mass flow rates of 1.67×10^{-2} and 1.67×10^{-1} kg/s in the stacked multi-channel at $t=4$s

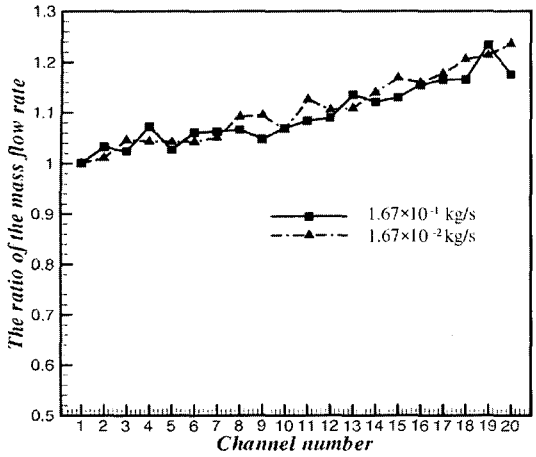

Fig. 15 Ratio of mass flow rate in the stacked multi-channel

ely uniform as shown in Fig. 15, compared to the case in the multi-branched multi-channel.

5. Conclusions

We carried out numerical studies to investigate the single- and two-phase flow characteristics in the single- and multi-channels using the finite volume method and VOF techniques. The present computational results are compared with the present experimental data, showing fairly good agreement both qualitatively and quantitatively.

The present computational results for the friction factor for the single-phase flow in the single-channel represent well the present experimental data and Moody chart. The phase interface between air and water for the two-phase flow in the single channel is developed from the irregular to the smooth shape as time goes on and the calculated time-averaged pressure drop for the two-phase flow in the single channel represents well the present measured data.

When the mass flow rate of water is small as 1.67×10^{-4}kg/s in the multi-branched multi-channel, the size of agglomerated air bubble is relatively uniform and is not large enough to block the flow of water-air mixture, resulting in the almost uniform mass flow rate through the multi-branched multi-channel. However, if the mass flow rate of water increases to 8.32×10^{-4} kg/s, the size of agglomerated air bubble becomes larger and blocks the mixture flow, resulting in the non-uniform mass flow rate through the multi-branched multi-channel. The ratio of mass flow rate in the stacked multi-channel is relatively uniform for different mass flow rates of 1.67×10^{-2} and 1.67×10^{-1} kg/s, compared to the case in the multi-branched multi-channel.

Acknowledgments

This works is partially supported by LG Electronics Co..

References

Alves, G. E., 1954, "Concurrent Liquid-Gas Flow in a Pipe-Line Contactor," *Chemical Engineering Progress*, Vol. 50(9), pp. 499~456.

Ashgriz, N. and Poo, J. Y., 1991, "FLAIR-Flux Line-Segment Model for Advection and Interface Reconstruction," *J. Computational Phys.*, Vol. 93, pp. 449.

Coleman, J. W. and Garimella, S., 1999, "Characterization of Two-Phase Flow Patterns in Small Diameter Round and Rectangular Tubes," *Int. J. Heat and Mass Transfer*, Vol. 42(15), pp. 2869~2881.

Elgobasi, S. E. and Abou-Arab, T. W., 1983, A Two-Equation Turbulence Model for Two-Phase Flows, Phys. Fluids, Vol. 26(4), pp. 931~938.

Hirt, C. W. and Nichols, B. D., 1981, "Volume of Fluid (VOF) Method for the Dynamics of Free Boundaries," *J. Computational Phys.*, Vol. 39, pp. 201~225.

Patankar, S. V., 1980, *Numerical Heat Transfer and Fluid Flow*, Hemisphere Publishing Co..